Image Cover Sheet

CLASSIFICATION	SYSTEM NUMBER
UNCLASSIFIED	503687

TITLE

HIGH-FREQUENCY REVERBERATION IN SHALLOW WATER

System Number:

Patron Number:

Requester:

Notes:

DSIS Use only:

Deliver to:

High-Frequency Reverberation in Shallow Water

Paul C. Hines and Dale D. Ellis, *Member, IEEE*

Abstract— **Monostatic reverberation measurements were collected in shallow water, over a coarse gravel and cobble bottom, 100 m deep, off the coast of Nova Scotia. Data were collected at frequencies of 21, 28, and 36 kHz using linear FM pulses of 2-kHz bandwidth and 0.160-s duration. An anchored, high-frequency active sonar array deployed at a depth of 42 m was used to collect the data. The reverberation measurements were compared with estimates computed with the NUWC generic sonar model (GSM). The data were reasonably well modeled for times greater than 0.2 s after pulse transmission by neglecting surface reverberation and using Lambert's rule for bottom backscattering with a scattering coefficient of −27 dB, independent of frequency. At all three frequencies, the data and model show a peak approximately 0.9 s after pulse transmission. This peak results from a focusing effect that the downward-refracting sound-speed profile has on the interaction of the rays with the bottom.**

Index Terms— **GSM, high frequency, reverberation, shallow water.**

I. Introduction

RECENTLY, there has been an increase in measurements of acoustic scattering at high frequency in shallow water environments (c.f. Jackson [1], Stanic [2], Ellis *et al.* [3], and references therein). These data, collected in conjunction with measurements of the physical properties of the bottom, are crucial if we are to fully understand the physics of acoustic scattering. Nonetheless, it is instructive to examine the problem from a more general system perspective as well. That is to say, can we model the prevalent features of shallow-water reverberation by employing a sonar system model such as the generic sonar model (GSM) [4]? To examine this issue, monostatic reverberation measurements were collected in water 100 m deep off the coast of Nova Scotia. The data were collected over the frequency band 20–40 kHz using a horizontally pointing sonar suspended to a depth of 42 m. In this paper, the averaged reverberation measurements are compared with modeled estimates obtained using GSM.

Following the introduction, we describe the experiment and the bottom topography of the experimental site. Then the reverberation data are presented and compared with estimates obtained using GSM. The most interesting feature in the data—a peak occurring at about 0.9 s after pulse transmission—is examined in light of the model results and the eigenrays interacting with the bottom. Finally, we present some conclusions.

II. Experimental Equipment and Geometry

Fig. 1 shows a schematic of the geometry for the reverberation experiment. The sonar array, named SEAHORSE, was deployed from the Defense Research Establishment Atlantic (DREA) research vessel CFAV QUEST, to a depth of 42 m. The seabed was nominally flat, with an average water depth over the extent of the experiment of 104 m. The benthic topography is discussed in greater detail in the following section. The experiment was conducted inside the perimeter of a tracking range developed and operated by US personnel. The tracking range allowed accurate positioning of SEAHORSE during the experiment.

SEAHORSE is an HF active sonar for collecting environmental acoustic data in the open ocean [5]. SEAHORSE was decoupled from surface motion using a two-stage decoupling system and anchored to the seabed within the tracking range using a second two-stage decoupling system. Although SEAHORSE was anchored, the decoupling system permitted some drift about the anchor. This drift was less than ±100 m during the experiment. The sonar operates over the frequency band 20–40 kHz. In conjunction with the acoustic sensors, SEAHORSE is instrumented with a range of nonacoustic sensors to assist in the evaluation of the data. The nonacoustic sensors include depth, tilt, roll, and heading sensors, to monitor array position and direction, as well as accelerometers to monitor platform motion. A series of motors contained in the sonar head point the sonar to the required azimuth and tilt. Communication between the research ship and SEAHORSE is handled via two RF links. The first is a one-way UHF data link which is used to transmit the acoustic and nonacoustic data collected by SEAHORSE back to the research ship, CFAV QUEST. The second is a two-way VHF command link which is used to maintain system control (e.g., select pulse type, set amplifier gains, control pointing direction, etc.).

The acoustic transmitter consists of a 48-element array of transducers, shaded such that one obtains an approximately conical beam of 0.1 sr, measured to the −3-dB points. (In cross section, this equates to a two-sided beamwidth of approximately 20°.) Fig. 2 shows the vertical and horizontal transmit beam patterns for a frequency of 28 kHz. Beam steering is accomplished mechanically. The sonar operates across the frequency band 20–40 kHz with a source strength of 202 ± 3 dB re 1 μPa @1 m. The same 48-element array used for the acoustic transmitter is used as the primary acoustic receiver. As a receiver, the 48-element array of transducers is shaded to obtain an approximately conical beam of 0.1 sr, measured to the −3-dB points. Fig. 3 shows the vertical and horizontal receive beam patterns for a frequency of 29 kHz. The receiver sensitivity is −180 ± 5 dB re 1 μPa/Hz across the frequency band 20–40 kHz.

III. Environmental Description

A. Benthic Topography

The site of the experiment was the eastern flank of the La Have Bank, about 100 nautical miles south of Halifax, Nova

Manuscript received June 6, 1996; revised January 7, 1997.

The authors are with the Defence Research Establishment Atlantic, Dartmouth, Nova Scotia, Canada B2Y 3Z7.

Publisher Item Identifier S 0364-9059(97)03398-0.

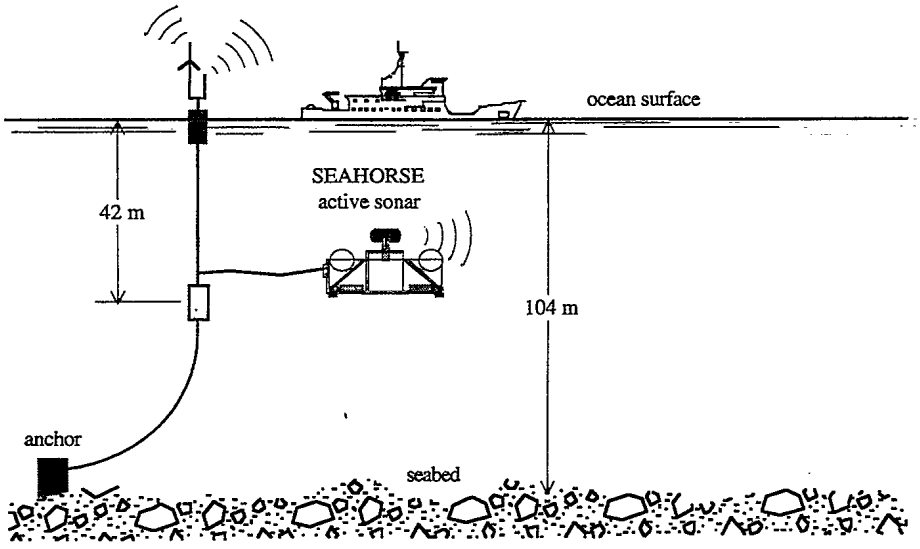

Fig. 1. Schematic of experimental geometry for reverberation experiment.

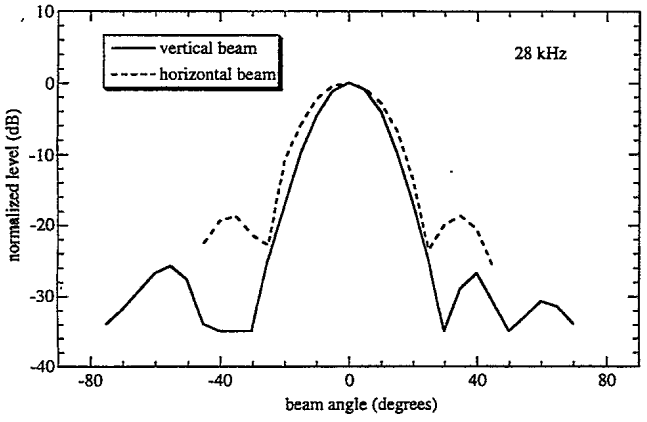

Fig. 2. The measured vertical and horizontal transmit beam patterns for a frequency of 28 kHz.

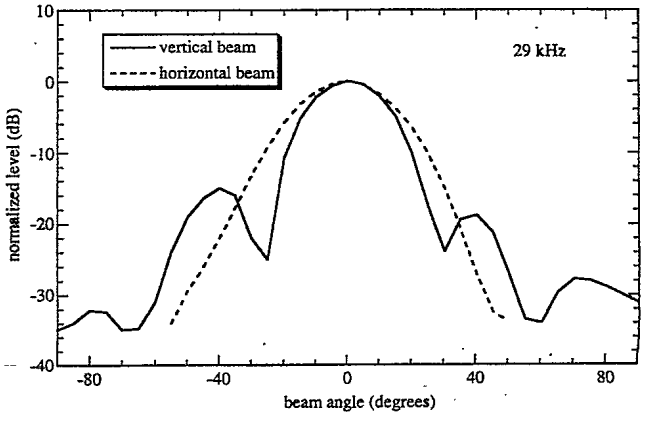

Fig. 3. The measured vertical and horizontal receive beam patterns for a frequency of 29 kHz.

Scotia, Canada. Fig. 4 shows a contour plot of the bottom for the experimental site. This contour plot was generated from bathymetric data collected with the CFAV QUEST bathymetric system. The bottom was surveyed on two occasions during the trial, once along north–south tracks separated by 500 m between tracks, and on a second occasion with north–south tracks separated by 200 m. A 5-s sampling interval provided samples along the tracks every 15 to 30 m. These data were combined to produce the set from which the contours were generated. As shown in the plot, the bottom had a gentle slope to the southeast, with the depth increasing from 100 to 110 m over about 10 km. Although there is little small-scale variability in the bathymetry, the bottom at the site is rough. Bottom mapping performed at the site [6] showed the bottom to be predominantly cobble, with the smoothest areas consisting of coarse gravel. There was a complete lack of fine-grained sediment at the site. Sidescan sonar records show a random distribution of highly reflective point sources interpreted to be boulders sized from 0.3 to 3 m. Several relict iceberg scours were distributed sparsely throughout the site. The coarse nature of the sediment resulted in no observable bottom penetration with a 3.5-kHz sub-bottom profiler. The sonar was pointed at an azimuthal angle of 345° ± 15° during the entire experiment. This corresponds to approximately up slope. The location of SEAHORSE is denoted in the figure by an X.

B. The Water Column

Fig. 5 shows sound-speed profiles taken at the site before (profile #21) and after completion (profile #22) the experiment. They are typical shallow-water summer profiles in the area: mixed surface layer, strong negative gradient, and sound channel. The minimum speed occurred at 42-m depth, coinciding approximately with the SEAHORSE depth. The sound-speed profiles, coupled with the depth of SEAHORSE, resulted in significantly more bottom interactions than surface interactions during the reverberation experiment. Fig. 6 shows the wind speed for a 24-h period commencing approximately 19-h prior to the experiment. The wind direction was reasonably steady from the southeast throughout the time period but increased in magnitude from about 1 m/s to about 12 m/s.

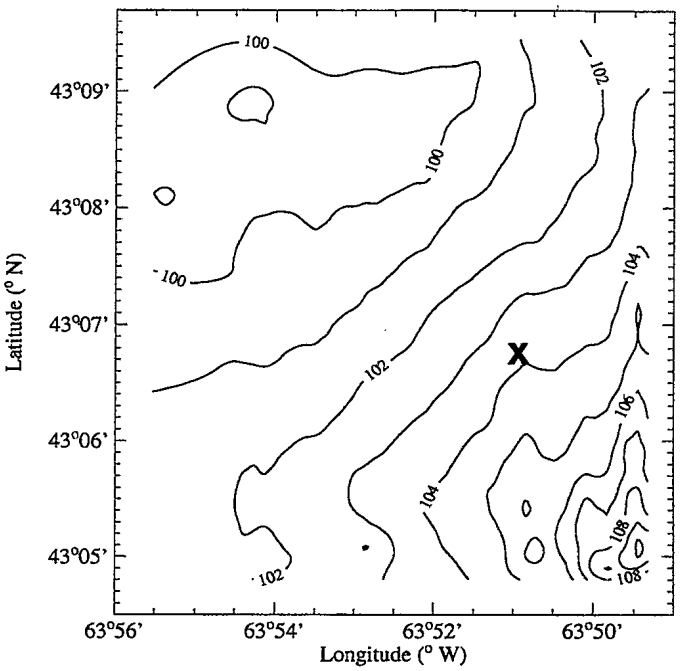

Fig. 4. Contour plot of the water depth (in meters) at the experimental site. The location of SEAHORSE during the experiment is denoted by an X.

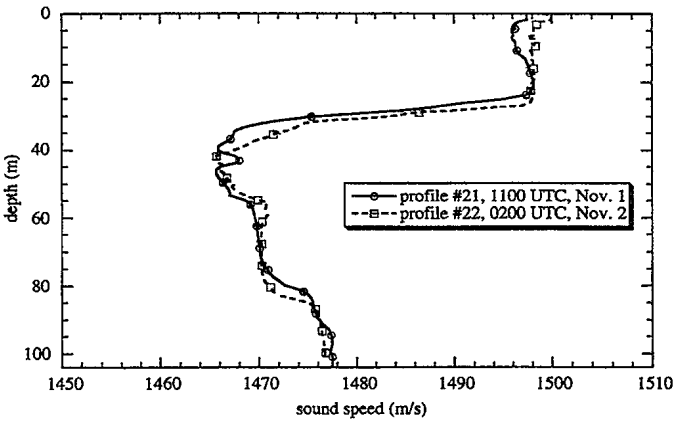

Fig. 5. Sound-speed profiles of the water column taken before (profile #21) and after completion (profile #22) of the experiment.

IV. The Reverberation Experiment

Three linear FM (LFM) pulse types were used during the reverberation experiment. Each of the three LFM pulses were 0.160 s in duration with 25% Tukey shading (12.5% at the start of the pulse and 12.5% at the end of the pulse). The three LFM's had 2-kHz bandwidths spanning frequencies of 20–22 kHz, 27–29 kHz, and 35–37 kHz, respectively. Throughout the remainder of this paper, each pulse type is referred to by its center frequency: 21, 28, or 36 kHz.

At each frequency, a sequence of 25 LFM pulses was transmitted with a pulse-to-pulse repetition rate of 15 s. For each transmitted pulse, data were recorded for approximately 4 s, starting about 240 ms prior to transmit. Synchronization dropouts in the data telemetry link—due to high seas—resulted in a loss of five to nine LFM pulses in each sequence.

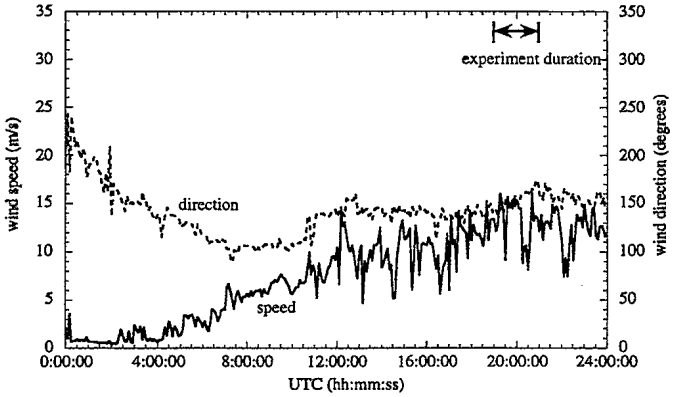

Fig. 6. Wind speed and direction for a 24-h period commencing approximately 19 h prior to the experiment.

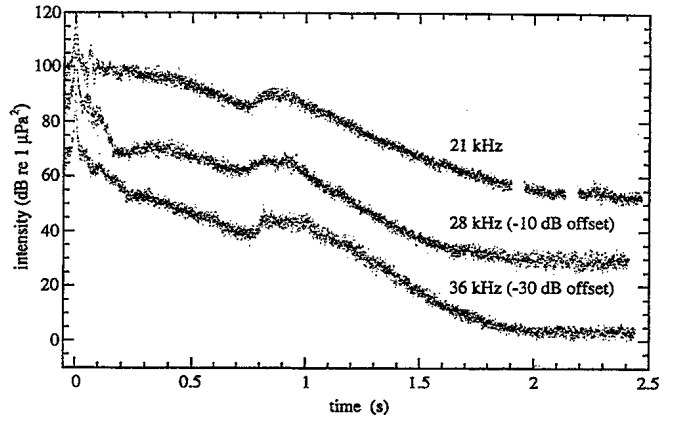

Fig. 7. Average intensity of the reverberation collected at three frequencies. The 28- and 36-kHz data are offset in the figure to prevent overlap of the three curves.

Analysis was performed on 16 pulses from each sequence so that the number of time series examined was consistent at all frequencies. During analysis, the pulses were heterodyned down in frequency to the band 500–2500 Hz, low-pass filtered, and subsampled by a factor of eight to reduce data processing and storage requirements. The time series recorded for each pulse was matched filtered in the frequency domain using fast convolution. Matched-filtering the data obtains a spatial resolution (to the −3-dB points) of approximately 0.4 m.

A. The Reverberation Measurements

Fig. 7 shows plots of the average intensity of the reverberation collected at 21, 28, and 36 kHz. The presence of a target in the water column contaminated the 21-kHz reverberation data at 1.9 and 2.2 s. Removing the target returns has resulted in the gaps in the 21-kHz curve. The 28- and 36-kHz data are offset in the figure to prevent overlap of the three curves. The peak at time $t = 0$ in all three curves results from electronic cross talk between the transmitter and the receiver during the transmission. The most interesting feature in the data is the local minimum at 0.8 s followed by the peak at approximately 0.9 s, at all three frequencies.

In the following section, we compare the reverberation measurements with results modeled using the GSM to gain some insight into the sources of the reverberation.

TABLE I
BOTTOM REFLECTION COEFFICIENT TABLE EMPLOYED FOR GSM CALCULATIONS

Grazing angle (degrees)	Bottom reflection coefficient (dB)
0.0	-0.00
2.0	-2.00
4.0	-4.00
6.0	-6.00
8.0	-8.00
10.0	-8.00
20.0	-8.00
90.0	-8.00

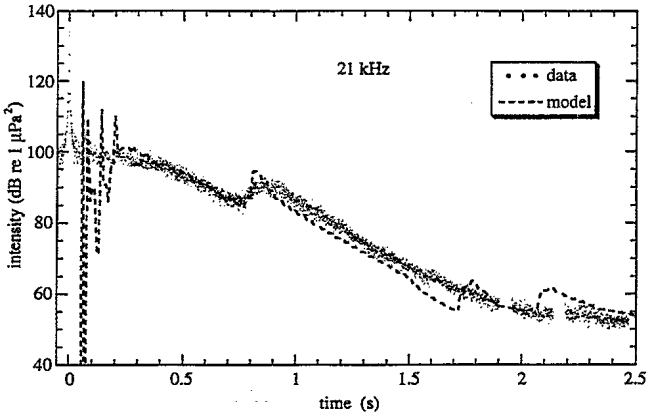

Fig. 8. Comparison of model estimates to the measured reverberation at 21 kHz.

V. COMPARISON OF REVERBERATION TO GSM

The reverberation measurements were modeled using GSM. The aim here is to examine the ability of a sonar system model to account for the prevalent features of shallow-water reverberation using literature estimates for the inputs. That is to say, how accurately can we interpret the measured reverberation with only limited environmental measurements available from the experiment? A comparison of the model to the data indicates that the surface reverberation does not contribute appreciably to the total reverberation. For now, we present this as a postulate and delay its verification until the discussion in Section V. Thus, the total modeled reverberation will consist of the sum of contributions from the bottom reverberation and the normal incidence reflections (henceforth referred to as fathometer returns).

Measured inputs to GSM included the transmit and receive beam patterns for SEAHORSE, sound-speed profile #22 from Fig. 5, and a wind speed of 25 knots. We assumed a pulse length of 0.67 ms to obtain a temporal resolution equivalent to that of the LFM pulses; the equivalent source level for use in GSM was increased by 28.3 dB to compensate for the shortened pulse length used in the model. The GSM submodel MULTIP (multipath expansion) was used to calculate the eigenrays at 100-m-range increments. Dahl's [7] empirically derived formula with a wind speed of 12 m/s was used to estimate the surface bubble loss. The bottom reflection coefficient was adjusted to fit transmission-loss data collected at the site. Table I contains the bottom reflection coefficients used in the model. However, the modeled bottom reverberation was not very sensitive to the choice of bottom reflection coefficient so that the agreement between data and model depends primarily on the bottom backscattering.

The bottom is described in [6] as rough gravel and cobble with virtually no penetration into the bottom. In addition, highly reflective point sources are distributed randomly throughout the region. At our frequencies, the gravel and cobble bottom can be considered very rough, so Lambert's rule for scattering should apply. Furthermore, Dyer *et al.* [8] has noted that a distribution of point scatterers can produce an average scattering that follows Lambert's rule. We shall use these heuristic arguments to invoke Lambert's rule [9] for the bottom backscatter model at shallow grazing angles. In addition to a backscatter model for shallow grazing angles, one normally applies a composite term to account for facet reflection at steeper angles (c.f. [10]). For our experiment, however, the facet contribution has virtually no effect due to the minimum in the transmit and receive beam patterns near vertical incidence (recall Figs. 2 and 3). Thus, for the present case, Lambert's rule should be sufficient to model the bottom backscatter.

The horizontal beam pattern was modeled simply as a 22° horizontal beamwidth (at all vertical angles). There is a correction [11] which would increase the reverberation at steep angles (short times). However, the correction is unimportant for the results shown here because the fathometer returns, beam pattern, and pulse transmission effects dominate the data at the steep angles.

A. Comparison of Modeled Reverberation to Measurements

Fig. 8 compares the modeled output at 21 kHz with the average intensity of the measured reverberation (replotted from Fig. 7). Several fathometer returns can be seen in the model, whereas only the first one is evident in the data. Furthermore, the model overestimates the intensity of the measured fathometer return. This is because the model output assumes a source level and temporal resolution which is constant at all times. However, for the first 0.16 s, there is actually a sliding source level and sliding resolution due to overload of the receiver during transmission. The dashed line is the bottom reverberation with a Lambert scattering coefficient of -27 dB and the model inputs described above. Lambert's rule appears to match the data reasonably well after about 0.2 s. The peak at 0.9 s occurring in the data is reasonably well modeled although the model overestimates the height-to-width ratio. The model also shows smaller peaks at 1.8 and 2.1 s not evident in the data. However, the data is approaching the ambient noise background and, as we shall show later, the amplitude of the modeled peaks is strongly influenced by the fine structure of the sound-speed profile.

Fig. 9 compares the modeled output at 28 kHz with the average intensity of the measured reverberation (replotted from Fig. 7). Lambert's rule with a coefficient of -27 dB matches

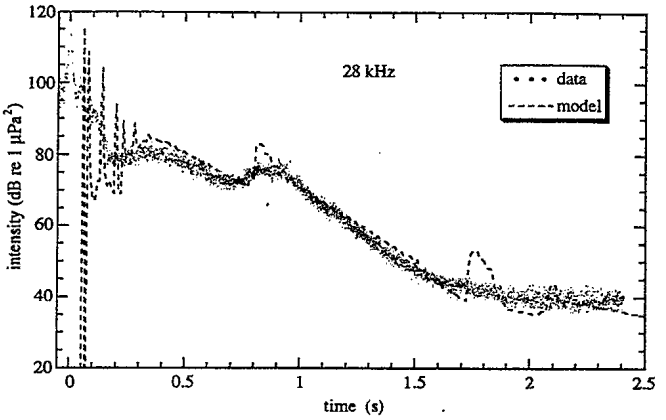

Fig. 9. Comparison of model estimates to the measured reverberation at 28 kHz.

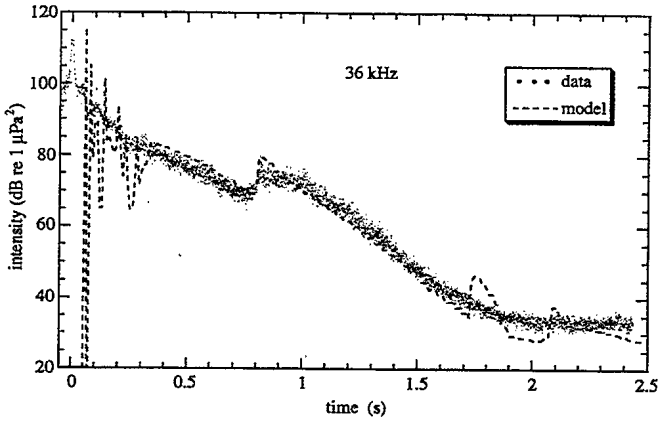

Fig. 10. Comparison of model estimates to the measured reverberation at 36 kHz.

the data reasonably well after about 0.2 s. The reverberation is lower than at 21 kHz, partly because of the lower source level, and partly due to the higher absorption in the water column at this frequency.

Fig. 10 compares the modeled output at 36 kHz with the average intensity of the measured reverberation (replotted from Fig. 7). Lambert's rule with a coefficient of −27 dB matches the data reasonably well after about 0.3 s.

VI. Discussion

The most interesting feature in the data is the peak which occurs at all three frequencies at approximately 0.9 s. If one were to examine only the data, this could easily be misinterpreted as a bottom feature. Clearly this is not so since the peak is accounted for in GSM—a flat-bottom model. In fact, the peak results from the refractive effects that the sound-speed profile has on the interaction of the rays with the bottom. This can be explained best with the aid of the eigenray diagram of Fig. 11. The figure shows the upgoing rays from −4° to −12° and the downgoing rays from 4° to 12°, in 1° increments, for 28 kHz. For clarity, the up-going rays are solid lines and the down-going rays are dashed. The rays departing at angles of −4° and 4° approximate the limits of the surface duct. Rays within these limits are trapped in the duct and

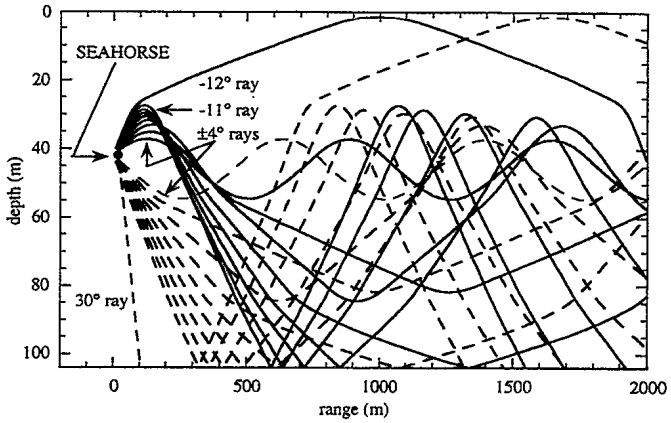

Fig. 11. Upward and downward rays for a frequency of 28 kHz to illustrate features in the reverberation.

are omitted from the figure. The up-going rays at −12° and −11° show the transition from surface reflection to refraction. Downgoing rays at angles steeper than 12° have been omitted for clarity; however, the first bottom interaction of the 30° ray is included to indicate the increase in ray density with increasing angle. The ray at 30° was chosen for this bound because 30° corresponds approximately to an arrival at 0.2 s, i.e., the end of the pulse transmission and data-overload region.

At intermediate angles of 30° to 9°, scatter of the downgoing direct path eigenrays dominate the reverberation (refer to Fig. 11). This corresponds to horizontal ranges of approximately 0.1–0.5 km. From approximately 0.5–1.3 km, the density of the downgoing eigenrays reduces drastically. This should result in a continuous decrease in reverberation. However, from about 0.6 to 0.9 km, refracted upgoing eigenrays interact with the bottom. These rays arrive in greater density and at steeper angles than do the downgoing rays. This causes the peak that occurs at 0.9 s. The peak that occurs in the model at 1.8 s results from a similar phenomenon. This time it is the bottom-reflected surface-refracted bottom-reflected (B-S-B) eigenrays which arrive at the bottom from 1.3 to 1.5 km in greater density than do the refracted upgoing eigenrays. Finally, the modeled peak at 2.3 s occurs because the surface-refracted bottom-reflected surface-refracted bottom-reflected eigenrays (S-B-S-B) begin arriving at the bottom at 1.55 km in greater density than the B-S-B eigenrays.

At all three frequencies, the model overestimates the amplitude while underestimating the width of the peak at 0.9 s. Furthermore, the model shows peaks at 1.8 and 2.3 s which do not appear in the data. Each of these discrepancies can be accounted for by a single phenomenon—fluctuations in the fine structure of the sound-speed profile. By way of example, Fig. 12 compares the modeled reverberation at 28 kHz for sound-speed profile #21 (recall Fig. 5) with the modeled reverberation for sound-speed profile #22. With the exception of the peaks, the modeled reverberation using the two profiles is virtually identical. The time and amplitude of the peaks, however, is strongly affected by what might appear to be minor differences in the sound-speed profiles. Clearly, at acoustic wavelengths of 4–8 cm, the fine structure of the sound-speed profile strongly influences the curvature

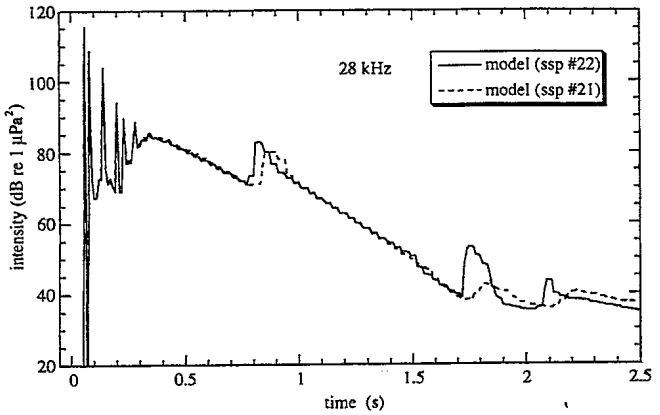

Fig. 12. Comparison of modeled reverberation at 28 kHz using profile #21 and profile #22 (from Fig. 5) to highlight the effect of the sound-speed profile on the peaks.

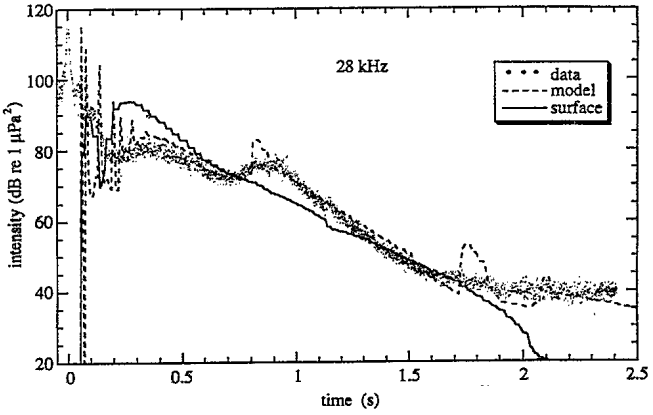

Fig. 13. Comparison of modeled surface reverberation with the modeled bottom reverberation and measured reverberation at 28 kHz.

of the eigenrays; this will determine the time of arrival and the amplitude of the peaks. Recall that 16 averages comprise the data at each frequency. Thus, even minute temporal or spatial fluctuations of the sound-speed profile will smear the peak in the measured reverberation. This would account for the broadening of the measured peak at 0.9 s. The amplitude of the peaks at 1.8 and 2.3 s are particularly dependent on the profile since they have upper turning points that are distributed more in range; their absence in the data is therefore not surprising.

We stated in Section IV that a comparison of the model and the data suggested that surface reverberation does not contribute appreciably to the total reverberation. The principal evidence of this derives from the agreement between the model and the data shown in Figs. 8–10—not the level of the data, which of course is set by the Lambert scattering coefficient, but its slope and most importantly, the peak occurring at 0.9 s. The only reasonable explanation of this feature is bottom reverberation. Our attempts to use GSM to model contributions from surface scatter removed all evidence of the peak in the data. Noting this, we feel justified in ignoring any contribution from surface reverberation. There is however, one point of concern; the limited published measurements of surface scattering in the frequency range of interest appear to overestimate our measured reverberation. Fig. 13 shows the data at 28 kHz along with our model (which ignores surface reverberation) and a surface reverberation calculation using surface scattering strength data collected in Dabob bay by Lilly and McConnell [12]. The data were published by McDaniel [13] in a review article. Clearly, the modeled surface reverberation overestimates the data for the first 0.9 s. However, the surface scattering strength values (from [13, Fig. 21]) were for the bubble saturation limit, which occurs above about 11 m/s. Prior to saturation, surface scattering will be reduced. Data are limited, but there is evidence [13, Fig. 22] that the bubble saturation limit in protected waters such as a bay have a much stronger wind-speed dependence than open-ocean measurements. This would result in lower surface scattering strengths in the open ocean than in protected waters for a given wind speed. [13, Fig. 22] shows that for a 15° grazing angle and a wind speed of 7 m/s, the surface scattering strength in the open ocean is lower by more than 15 dB. Clearly, a reduction of 15 dB in the modeled surface reverberation would render the surface contribution shown in Fig. 13 unimportant. Although the wind speed during our (open-ocean) experiment was approximately 12 m/s, the winds had been increasing steadily (from near 0 m/s) throughout the day, and it is conceivable that the seas had not developed to the point of bubble saturation.

The Lambert coefficient of −27 dB could be adjusted slightly to provide improved model-data agreement in Figs. 8–10: −25 dB at 21 kHz, −29 dB at 28 kHz, and −27 dB at 36 kHz. However, given the various uncertainties, this degree of tuning may not be justified. One should note that these values are several decibels lower than those typical of rough, cobble bottoms (c.f. [14] and references therein). Nonetheless, Wong and Chesterman [15] measured values for the Lambert coefficient for rock bottoms that ranged from −12 to −25.5 dB.

VII. Summary and Conclusion

High-frequency reverberation measurements were collected with an active sonar array deployed in shallow water 100 m deep off the coast of Nova Scotia. Data were collected at center frequencies of 21, 28, and 36 kHz using LFM pulses 0.16 s in duration with a 2-kHz bandwidth. At each frequency, monostatic reverberation measurements obtained from averaging the returns from 16 pings were compared with estimates computed with the GSM. GSM inputs were estimated from the literature using a limited amount of environmental data measured at the site.

Based on the measured slope and features shown in the data, it appears that contributions from surface reverberation can be ignored in the model. Furthermore, a limited set of published measurements appears to lend support to this assumption.

The measured data were reasonably well modeled for times greater than 0.2 s after pulse transmission using Lambert's rule with a scattering coefficient set to −27 dB independent of frequency. At all three frequencies, the data and model exhibit a maximum approximately 0.9 s after pulse transmission. This results from the effect that the sound-speed profile has on the

interaction of the eigenrays with the bottom, i.e., it is not a bottom feature but an effect resulting from ray curvature.

ACKNOWLEDGMENT

The authors wish to acknowledge the valuable discussions with A. J. Collier of the Defence Research Establishment Atlantic (DREA). Furthermore, the authors wish to acknowledge the contributions of the experimental team from DREA, as well as R. L. Culver and the experimental team from The Applied Research Laboratory, The Pennsylvania State University, and The Applied Research Laboratory, Keyport, WA, and D. Jepsen and the experimental team from NUWC-Keyport. The authors also wish to acknowledge NUWC for release of GSM to DREA.

REFERENCES

[1] D. R. Jackson, A. M. Baird, J. J. Crisp, and P. A. G. Thomson, "High-frequency bottom backscatter measurements in shallow water," *J. Acoust. Soc. Amer.*, vol. 80, pp. 1188–1199, 1986.

[2] S. Stanic, K. B. Briggs, P. Fleischer, R. I. Ray, and W. B. Sawyer, "Shallow-water high-frequency bottom scattering off Panama City Florida," *J. Acoust. Soc. Amer.*, vol. 83, pp. 2134–2144, 1988.

[3] D. D. Ellis, J. R. Preston, and H. G. Urban, Eds., *Ocean Reverberation*. Dordrecth, The Netherlands: Kluwer, 1993, sect. 2.

[4] H. Weinberg, "The generic sonar model," Tech. Document 5971D, Naval Underwater Systems Center, New London, CT, 1985.

[5] P. C. Hines, J. S. Hutton, and A. J. Collier, "A free floating, steerable, HF sonar for environmental measurements," in *IEEE Oceans'93 Conf. Proc.*, 1993, vol. 2, pp. 65–70.

[6] G. Gilbert, D. Hutton, and P. Campbell, "Seabed mapping for DREA experimental sites," Defence Research Establishment Atlantic Contractor Rep., DREA CR/96/404, 1996.

[7] P. H. Dahl, "Bubble attenuation effects in high-frequency surface forward scattering measurements from FLIP," APL-UW TR 9307, Applied Physics Laboratory, University of Seattle, WA, 1993.

[8] I. Dyer, A. B. Baggeroer, H. Schmidt, J. R. Fricke, N. Ozluer, and D. Giannoni, "Discrete backscatter can be dominant in rough bottom reverberation," in *Ocean Reverberation*, D. D. Ellis, J. R. Preston, and H. G. Urban, Eds. Dordrecht, The Netherlands: Kluwer, 1993, pp. 51–57.

[9] K. V. MacKenzie, "Bottom reverberation for 530 and 1030-cps sound in deep water," *J. Acoust. Soc. Amer.*, vol. 33, pp. 1498–1504, 1961.

[10] D. R. Jackson, D. P. Winebrenner, and A. Ishimaru, "Application of the composite roughness model to high frequency bottom backscattering," *J. Acoust. Soc. Amer.*, vol. 79, pp. 1410–1422, 1986.

[11] D. D. Ellis, "Effective vertical beam patterns for ocean acoustic reverberation calculations," *IEEE J. Oceanic Eng.*, vol. 16, pp. 208–211, 1991.

[12] J. C. Lilly and S. O. McConnell, "Surface reverberation measured in dabob bay and the open ocean," *J. Acoust. Soc. Amer.*, vol. 63, suppl. 1, p. S24, 1978.

[13] S. T. McDaniel, "Sea surface reverberation: A review," *J. Acoust. Soc. Amer.*, vol. 94, pp. 1905–1922, 1993.

[14] R. J. Urick, *Principles of Underwater Sound*, 2nd ed. New York: McGraw-Hill, 1975, pp. 243–250.

[15] H.-K. Wong and W. D. Chesterman, "Bottom backscattering near grazing incidence in shallow water," *J. Acoust. Soc. Amer.*, vol. 44, pp. 1713–1718, 1968.

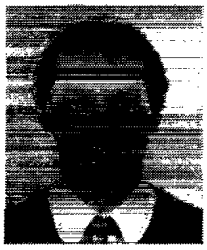

Paul C. Hines was born in Glace Bay, Nova Scotia, Canada, in 1958. He received the B.Sc. (Hon.) degree in engineering physics from Dalhousie University, Halifax, Canada in 1981 and the Ph.D. degree in physics from the University of Bath, U.K. in 1989.

From 1981 to 1985, he was a Scientist in the Sonar Projects group at the Defence Research Establishment Atlantic (DREA), working in the field of towed array self-noise. Upon returning from the University of Bath in 1989, he joined the Acoustic Countermeasures group at DREA to work on scattering and time spreading. Presently, he is Leader of the Airborne Sensors group at DREA. His present research interests include acoustic scattering and frequency and time spreading spreading.

Dr. Hines is a member of the Acoustical Society of America.

Dale D. Ellis (M'92) was born in Bathurst, New Brunswick, Canada, in 1949. He received the B.Sc. degree in mathematics and physics from Mount Allison University, Sackville, NB, in 1970 and the M.Sc. and Ph.D. degrees in theoretical nuclear physics from McMaster University, Hamilton, Ontario, in 1971 and 1976, respectively.

Since 1977, he has been employed at the Defence Research Establishment Atlantic in Dartmouth, Nova Scotia, Canada, and is currently Leader of the Modeling and Systems Analysis Group. From 1990 to 1994, he was a Scientist at the SACLANT Undersea Research Centre in Italy. His main research efforts have been in numerical modeling of shallow-water propagation and scattering, and comparisons with data. His current emphasis is on rapid environmental assessment.

Dr. Ellis is a fellow of the Acoustical Society of America and a member of the Canadian Acoustical Association, the Canadian Applied Mathematics Society, and the Royal Astronomical Society of Canada.

#803687